J Solid State Electrochem (2005) 9: 535–546
DOI 10.1007/s10008-004-0587-9

ORIGINAL PAPER

S. Velumani · H. Castaneda · U. Pal · J. A. Chavez
P. J. Sebastian · J. A. Ascencio

Structural and electrochemical characterization of sputter-deposited nitrided NiCr alloys

Received: 17 February 2004 / Revised: 8 March 2004 / Accepted: 5 August 2004 / Published online: 18 March 2005

Abstract Nickel-based coatings are potential candidates for the protection of electrochemical dissolution of steel surfaces. Such coatings, elaborated by magnetron sputtering in a nitrogen atmosphere, offer good corrosion protection, good adherence as well as stability for metallic structures. NiCr alloys with almost constant composition have been deposited with different nitrogen contents on stainless steel and carbon steel surfaces. The coating uniformity, homogeneity, composition and crystallinity have been studied by scanning electron microscopy, energy-dispersive X-ray spectrometry, atomic force microscopy and X-ray diffraction techniques. The corrosion degradation behavior of all the samples was tested in NaCl and NaCl and CO_2 mixture exposures using electrochemical impedance spectroscopy measurements. Nitrided NiCr alloys on a stainless steel substrate resulted with better adhesion than carbon steel, by delaying the corrosion mechanism when exposed to NaCl and CO_2 solution. A comparison of the corrosion resistive behavior of the substrates (stainless steel, carbon steel) and the coatings is made by using the electrical capacitance concept from a double-layer model for the coating–metal interface.

S. Velumani · H. Castaneda · J. A. Ascencio (✉)
Programa de Investigación y Desarrollo de Ductos,
Instituto Mexicano Del Petróleo, Eje Central Lázaro Cárdenas,
C.P. 07730 Mexico D.F., Mexico
E-mail: ascencio@imp.mx
Tel.: +52-55-91758055
Fax: +52-55-91756429

U. Pal
Instituto de Física, Universidad Autónoma de Puebla,
Apdo. Postal J-48, Pue, 72570, Mexico

J. A. Chavez
IIM, Universidad Nacional Autónoma de México,
Circuito Exterior, C.U.,
C.P. 04510 Mexico D.F., Mexico

P. J. Sebastian
CIE-Universidad Nacional Autónoma de México,
Temixco, Morelos, 62580, Mexico

Keywords NiCr coatings · Electrochemical methods · Corrosion · Surface analysis

Introduction

Most industries are faced with the challenge of protecting products from corrosion and its degradation effects. Nickel is largely used as a construction material in the process industry owing to its fair resistance towards common corrosion. In the last decade much attention was devoted to the study of the physical and electrical properties of NiCr thin films [1–5]. Alloying with Cr leads to a significant decrease of the susceptibility of Ni towards localized corrosion. Because of this, Ni–Cr alloys are widely used as welding materials for highly alloyed steels in oxidizing conditions. Alloying of Ni with Cr, however, can lead to an increased susceptibility to common corrosion in highly oxidizing environments via transpassive dissolution of Cr. These films are also very interesting in microelectronics owing to their applications in thin-film resistors, potentiometers, fusible links, read-only memories, etc. [6–8]. Especially the fuel cell industry is facing a major challenge in developing lightweight metallic bipolar plates and protective coatings with high corrosion resistance and high conductivity. Many surface treatments are realized by various techniques, like wet chemical or electroless processes and electrodeposition. These treatments satisfy the usual conditions of corrosion resistance and cost. Nevertheless, the functional corrosion resistance of the coatings may be insufficient with regard to the requirements of increasing performance. Moreover, these surface treatments are more subject to restriction or regulation because of their harmful environmental effects. New material combinations, alloyed in a different atmosphere by vacuum deposition, are extending the potentials of techniques like sputtering for mechanical (machining, wear protection) and protective (corrosion, oxidation) applications. Among the deposition

techniques, sputtering appears to be an interesting and promising way to deposit corrosion-resistant coatings, as apart from the environmental friendly character, it allows generally dense, adherent and pure deposits.

The electrochemical behavior of pure Ni in neutral and alkaline environments has been studied with different techniques, such as electrochemical impedance, and potentiostatic electrochemical methods [9, 10] in order to characterize the film stability of metallic oxides that formed when Ni was exposed in different pH conditions. Also studies such as on the role of hydrogen on adhesion on NiCr by spray coating [11] and adhesion of nanocrystalline Ni–Fe alloys [12] have been reported. However, the results for the structure of the passive film are controversial. Some authors have reported the film consists of NiO [13–16], but most researchers have aligned themselves with the duplex structure of either NiO and $Ni(OH)_2$ [17–20] or NiO and Ni_3O_4 [21]. The oxidation of divalent to trivalent nickel leading to the formation of an oxyhydroxide (NiOOH) at high potentials in the transpassive region has been reported in many articles [14, 18, 20, 22]. On the other hand, there are reports of the formation of three different oxides (NiO and two unassigned oxides) in the transpassive region. In situ potential modulated reflection spectroscopic studies [23] have indicated that the passive film formed in neutral solutions consisting mainly of NiO, with a possible contribution of a nonstoichiometric NiO_x oxide in the outermost part of the film. The value of x, which is related to the excess oxygen content due to the presence of trivalent nickel ions, was thought to increase with increasing potential [23]. Sato and Kudo [15] have suggested on the basis of ellipsometric measurements that the film forming at very high potentials during secondary passivation is composed of Ni_2O_3.

Considering steel corrosion, nitrided nickel-based coatings may ensure a good protection which has not been explored thoroughly. Hence in this work, we conducted a systematic investigation on nitrided NiCr alloy films prepared by rf reactive magnetron sputtering using a composite NiCr target. Nitrided NiCr films on the carbon steel and stainless steel substrates were obtained and a detailed analysis of the structural and electrochemical characterizations was performed and is reported. The crystal structure, surface morphology, composition and electrochemical analysis in the NaCl and CO_2 atmosphere were carried out to test the corrosion protection behavior of the films and the effect of surface morphology on it.

Experimental procedure

Nitrided NiCr thin films were deposited by rf magnetron sputtering at room temperature. A NiCr composite metal target (99%, 2-in. diameter, Ni to Cr ratio of 80:20, Good Fellow, Cambridge, UK) was sputter-deposited on well-polished stainless steel and carbon steel substrates with 100-W sputtering power at 20 mTorr Ar/N_2 gas pressure for 3 h. Prior to deposition, the mirror-polished substrates were cleaned chemically (vapor degreasing, ultrasonic cleaning and rinsing in alkaline solution and water) and the sputter was cleaned using an argon plasma for 10 min. For sputtering, ultra-high-purity argon and nitrogen (99.999%) gases were used. The films were deposited for different ratios of 2:8, 4:6 and 8:2 of nitrogen and argon gas mixtures in the chamber. The thickness of the films was measured using a Dektak II profilometer. The crystal structure of the films was determined using a Bruker AXS D8 Advance diffractometer (X-ray diffraction, XRD) with a graphite monochromator and Cu Kα ($\lambda = 0.154056$ nm) radiation. The surface morphology, composition and elemental mapping of the films were analyzed using a JEOL JSM 6400 scanning electron microscope (SEM) coupled with a Noran energy-dispersive X-ray analytical system. For the topographical analysis of the samples, an SPM Nanoscope4 atomic force microscope system (from Digital Instruments) was used in contact mode.

Electrochemical experiments for the Ni/Cr coated substrate was performed by impedance spectroscopy in the frequency range from 20 kHz to 100 MHz at a constant amplitude of 10 mV. A three-electrode rectangular cell setup (Fig. 1) was designed to handle the samples easily and to study the electrochemical behavior of different samples. CO_2 gas was injected into the cell up to 100 ppm of CO_2, in solution, by changing the exposure time of the gas injected into the electrolytic solution. CO_2 dissociates into HCO_3^- and CO_3^{2-}, which are ions that acidify the electrolyte in the pores of a surface exposed in electrolytic conditions [16].

The 3% NaCl and the 3% NaCl and CO_2 (100 ppm dissolved) mixtures were used as electrolytes. For electrochemical testing a 0.7-cm^2 area of the deposited film was exposed and this acted as a working electrode; a graphite rod was the counter electrode and a saturated calomel electrode was the reference electrode.

Results and discussion

Structural and surface morphological analysis

It is well known that the microstructure plays a predominant role in determining the behavior of materials in several applications. Therefore, the control and optimization of microstructure is very important for materials in thin-film form for any of their applications. Several processing techniques, including sputtering, are very effective for producing uniform microstructures with uniform and dense coatings. Metallographic microscopic observations revealed that the coatings are usually free from porosity, oxides, semimelted and un umelted particles, and inclusions, which are commonly observed in other chemical depositions techniques.

Figures 2 and 3 show the typical XRD patterns of the nitrided NiCr coatings of about 1.2-μm thickness

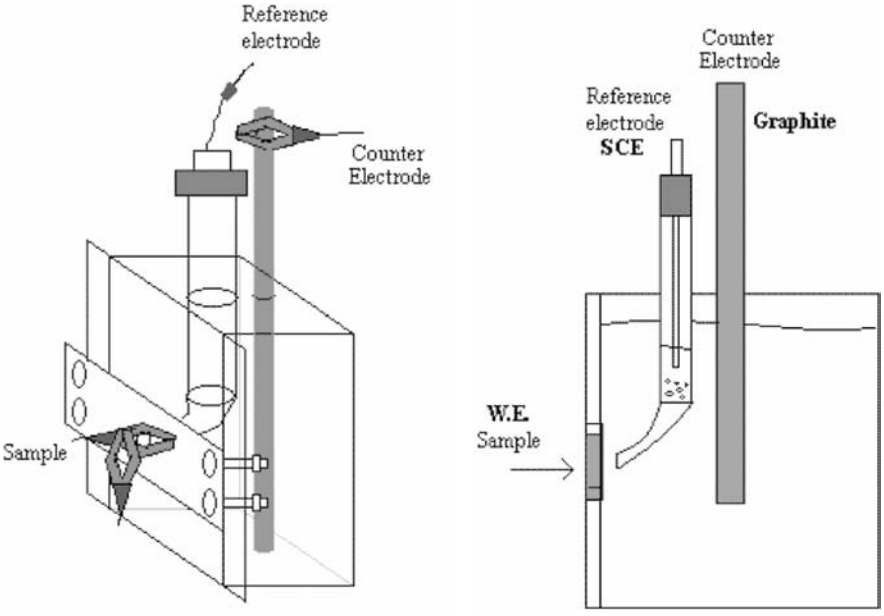

Fig. 1 Typical three-electrode cell system with adjustable working electrode. A graphite rod is used as a counter electrode and a saturated calomel electrode is the reference for controlled open circuit potential magnitude and impedance measurements

produced by sputtering on the carbon steel and the stainless steel substrates. The structure of the films was analyzed using an X-ray diffractometer. The line profiles were subjected to variance analysis and, since the method is sensitive to variation near the tails of the peaks, a careful adjustment of the background was carried out. Also the profiles were corrected for instrumental broadening by subtracting the variance of the corresponding profile from a standard source. The crystallite sizes (D) were calculated using the Scherrer formula [24] from the full width at half maximum (β):

$$D = \frac{0.94\lambda}{\beta \cos\,\theta}. \tag{1}$$

The strain (ε) was calculated from the slope of the $\beta\cos\theta$ versus $\sin\theta$ plot using the relation [25]

$$\beta = \frac{\lambda}{D\cos\,\theta} - \varepsilon \tan\,\theta. \tag{2}$$

The dislocation density (δ), defined as the length of the dislocation lines per unit volume of the crystal, was evaluated from the formula

$$\delta = \frac{1}{D^2}. \tag{3}$$

From Table 1 it can be observed that there is a slight increase in the crystallite size with the decrease in the

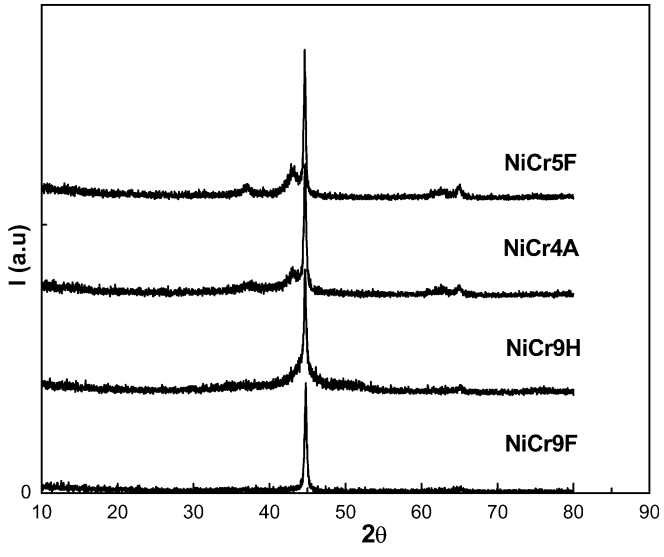

Fig. 2 X-ray diffraction (*XRD*) spectra of the NiCr alloy films deposited on carbon steel substrates

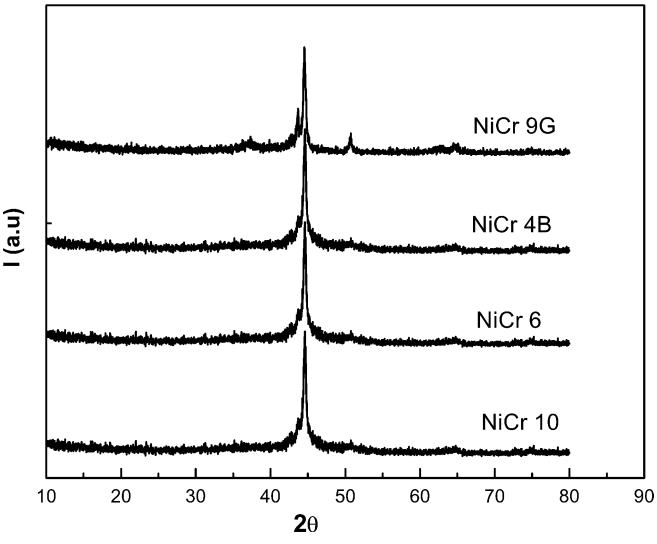

Fig. 3 XRD spectra of the NiCr alloy films deposited on stainless steel substrates

Table 1 Variation of microstructural parameters of the NiCr films prepared at different nitrogen/argon gas flow rates on carbon steel and stainless steel substrates

Sample	N_2/Ar flow	Nitrogen (atom %)	Chromium (atom %)	Nickel (atom %)	d (nm)	D (nm)	δ (10^{14} lin m^{-2})	ε (10^{-4} lin^{-2} m^{-4})
Carbon steel								
NiCr5F	60/40	10.22	19.02	70.76	2.0303	28.28	12.50	19.46
NiCr4A	50/50	8.21	19.46	72.33	2.0284	31.01	10.39	17.54
NiCr9H	40/60	7.06	19.97	72.97	2.0307	32.74	9.32	15.62
NiCr9F	20/80	5.76	19.7	74.55	2.0382	33.35	8.99	9.29
Stainless steel								
NiCr4B	60/40	11.67	29.66	58.67	2.0323	25.59	15.27	18.52
NiCr9G	50/50	9.36	28.24	62.40	2.0321	25.68	15.16	15.38
NiCr10	40/60	7.35	27.56	65.09	2.0313	27.17	13.54	10.67
NiCr6	20/80	5.47	26.32	68.21	2.0353	28.28	12.50	8.42

nitrogen content both on the carbon steel and on the stainless steel. Since crystallite size and dislocation density are inversely related, the dislocation density decreases with increase of the crystallite size. It is also found that the strain increases with the increase in nitrogen content on both the carbon steel and the stainless steel substrates, substantiating the breakdown mechanism in the electrochemical studies.

A SEM micrograph of the NiCr coatings on the stainless steel substrate is shown in Fig. 4 and it depicts a very smooth surface morphology. Similar surface morphology was also observed for the NiCr-coated carbon steel substrates. The coatings are regular, with columnar but relatively dense structure.

By using atomic force microscopy (AFM), the surface topography of the NiCr films along with the substrates was studied (Fig. 5). Similar measurement conditions were maintained for all the samples in order to have comparable data. The basic study comprised a 3D representation and the section analysis method that allows determination of the profile of the sample with a line drawn over the surface (Fig. 5b). On the uncoated steel surface, we can identify the effects of the mechanical polishing as linear marks (channels thereafter) and small clusters along with small fragments of the materials of

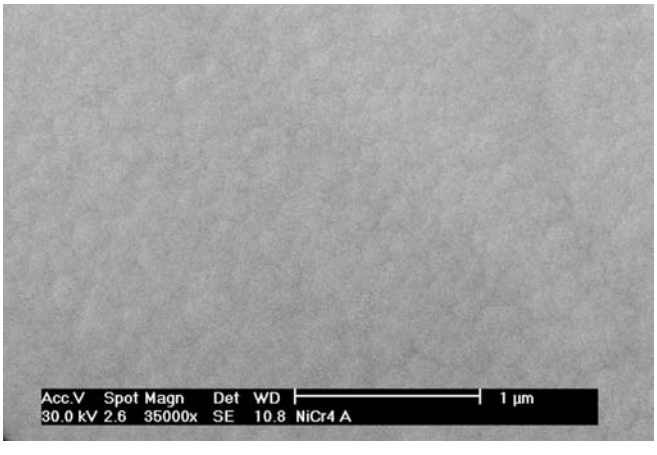

Fig. 4 A typical scanning electon microscope image of the nitrided NiCr coatings on the stainless steel substrates

less than 20 nm. However, the depths of the observed channels are really small (around 80 nm) as can be observed in the profiles along with further smaller channels of around 5-nm depth.

After the deposition of nitrided NiCr alloys on these substrates, the morphology changed dramatically and continuous small clusters covering the entire surface were produced. The topography is found to be more regular and the channels and valleys observed on the substrates were carried over after the coating, with large changes in the height. Figure 6 shows the AFM image of a nitrided NiCr coating on the stainless steel substrate obtained in tapping mode. From this 500-nm scan study we can identify the formation of small clusters of material on the order of tens of nanometers, covering the entire surface and forming a very smooth surface without any pronounced changes in the height of the coating. It is clearly evident that this is the effect of the nitrided NiCr coating over the surface and in the 3D representation, which has a height scale of 30 nm and the three section profiles, allows the determination of the highest clusters of around 30 nm. With the help of the section analysis, the profile is also well understood and we can study the size distribution of the clusters, which are between 20 and 30 nm, with most of them around 30 nm, almost exactly coinciding with the crystallite size evaluated from the XRD pattern (Table 1). It is interesting to observe that the even very smaller clusters of around 10 nm are present in the valley regions of the sample, as clearly depicted in the 3D image (Fig. 6). Also in the profile we can identify the flatter sections at the top of the surface, with bigger clusters, which may be due to the agglomeration of smaller particles. Also high-magnification images of the flat section of the surface revealed very smooth boundaries between clusters/grains even for their larger height differences. In the 3D image it is evident that the domains are produced with localized high-energy zones of boundaries, which are usually considered to be the promoters of cracking or preferential zones for corrosion to start; this is substantiated in the last section using the SEM analysis of the corroded surfaces.

A similar AFM study on the carbon steel (Fig. 7) substrates revealed that the carbon steel substrates are rather smooth in topography with no predominant

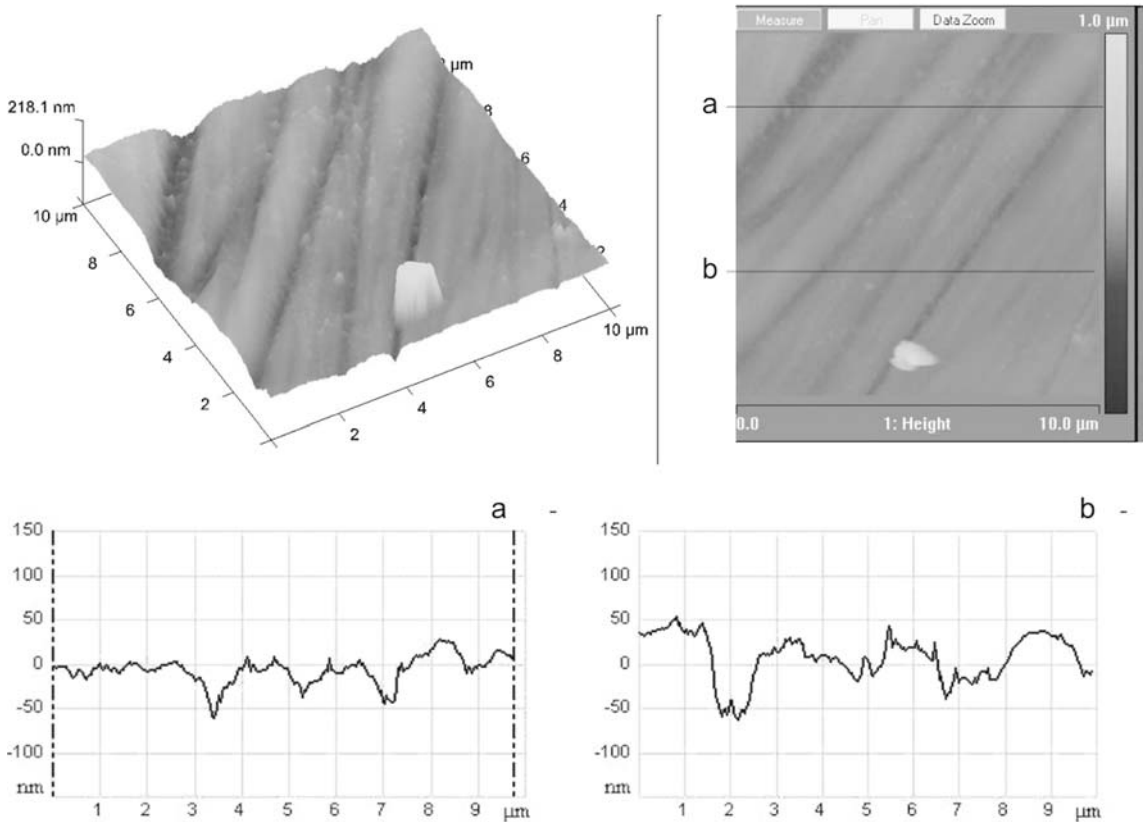

Fig. 5 Atomic force microscopy (*AFM*) image of the bare stainless steel substrate surface depicting channels and small clusters produced by mechanical polishing

channel structures as observed in the case of stainless steel substrates. There are some shallow valleys of around 3-nm depth and the phase-contrast AFM images revealed no corrosion on these substrates due to air oxidation.

The NiCr films deposited on stainless steel substrates posses smooth topography with an average height variation of about 10–15 nm only. Phase-contrast AFM images revealed no composition inhomogeneity in the films. In the early stages of corrosion, the nitrided NiCr coatings did not reveal any drastic change in topography in comparison with the uncorroded samples. However, by phase-contrast AFM imaging, it was possible to locate the zones affected by corrosion.

From Fig. 7 we could identify the corrosion-affected zones of around 40-nm×10-nm area surrounded by the grain boundaries. The corrosion process seems to be favored on the grain boundaries and it is similar in the case of the nitrided NiCr films grown on carbon steel substrates. However, the process appears to be strongly dependent on the topography of the coated surface.

Composition analysis

The composition analysis was performed for one representative film from each set of the films prepared under different conditions (different nitrogen flows). From Table 1 it is clearly evident that when the nitrogen flow rate increases, the incorporation of N_2 in the films is high. Even though the deposition conditions were maintained the same for the carbon steel and stainless steel substrates, for all the films deposited on carbon steel substrates, the composition of the target is almost maintained, whereas, for the deposits on the stainless steel substrates, the chromium contents are found to be higher.

Electrochemical impedance spectroscopy

The characteristic impedance spectra for the NiCr films deposited on carbon steel substrates exposed to 3% NaCl solution (pH 7.4) are presented in Fig. 8. The Nyquist or complex diagram shows that the interface between coating and electrolyte is described by means of electrochemical and transport phenomena processes. Coating wetability and interaction with the environment can be illustrated in terms of two different electrical equivalent circuits for the interface that characterize the surface behavior in 3% NaCl, as illustrated in Fig. 8. Mansfeld and Tsai [27] described an equivalent circuit as illustrated in Fig 8a, where the steel coating system has two different contributions from the interfaces formed, one contribution due to the coating and the second due to the outer interface between the coating and the electrolyte.

The model represents a resistance R_s that follows the solution resistance in Fig. 9a. C_c is the coating

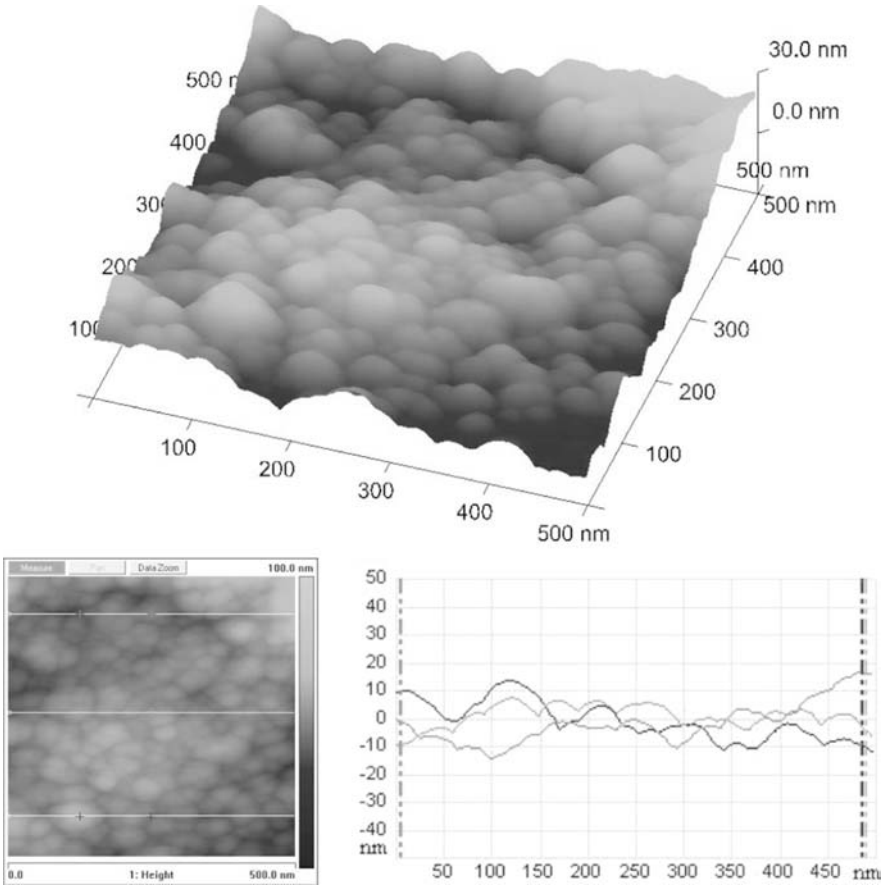

Fig. 6 AFM images of the surface of stainless steel substrates after nitrided NiCr film deposition depicting the formation of grains, and the section analysis showing grain size variations around 20–30 nm

capacitance subjected to ionic interaction, the metal surface with electrolytic solution, R_{po} is the coating resistance (pore resistance), C_{dl} is the capacitance at the area under the coating where dissolution exists, and R_{ct} is the charge transfer resistance associated with the electrochemical reactions and metallic dissolution owing to faradic processes. The impedance spectra for the NiCr9H and NiCr9F samples show the best corrosion resistance. Table 2 shows the various values of R_s, R_{ct}, C_{dl}, R_{po} and C_c evaluated for different films. From these values and the impedance spectra, it is explicit that samples NiCr9H and NiCr9F show the best corrosion resistance among the various carbon steel substrate coatings. From Table 2 open circuit potentials (OCP) of magnitudes −0.44 and −0.49 V versus the saturated calomel electrode (SCE) are estimated for NiCr9H and NiCr9F, respectively. The complex diagram shows a mass-transfer phenomenon, where a semicircle at high frequencies showed in Fig. 8a (inset) a local maximum at 961 Hz, which is attributed to the coating impedance or ionic diffusion into the substrate from the solution. At lower frequencies the magnitude of the charge transfer resistance can be obtained from extrapolation of the lowest-frequency point in Fig. 8a, where a second semicircle is formed. NiCr5F and NiCr4A show semicircles along the frequency spectra, describing an active surface and the OCP (Table 2) denotes a more active surface for NiCr5F and NiCr4A with −0.673 and −0.591 V versus the SCE, respectively.

Bare carbon steel shows an OCP of −0.684 V versus the SCE and has an active surface; this behavior is corroborated in the Nyquist representation with a semicircle form in Fig. 8. The magnitude of R_{ct} is associated with the surface dissolution of the substrate material. Impedance spectra for this coating are characteristic of a charge transfer control process, where the diameter of the semicircle in the Nyquist plot is related to the substrate dissolution process. Therefore, the bigger the semicircle the higher will be the corrosion resistance.

Figure 10 shows phase angle magnitudes at different frequencies for each coating on the carbon steel substrates. This representation shows one or more time constants controlling the interfacial mechanism. NiCr9H and NiCr9F samples represent three time constants that correlate the response described previously in the complex representation; both samples at high frequency show a maximum point or time constant, attributed to a constant phase element (CPE) that considers a pseudo-capacitance formed because of the coating layer. Medium-range frequencies correspond to a second time constant, which is attributed to the double-layer capacitance, and the third time constant corresponds to the lowest-frequency point or the charge transfer magnitude. NiCr5F, NiCr4A and bare steel

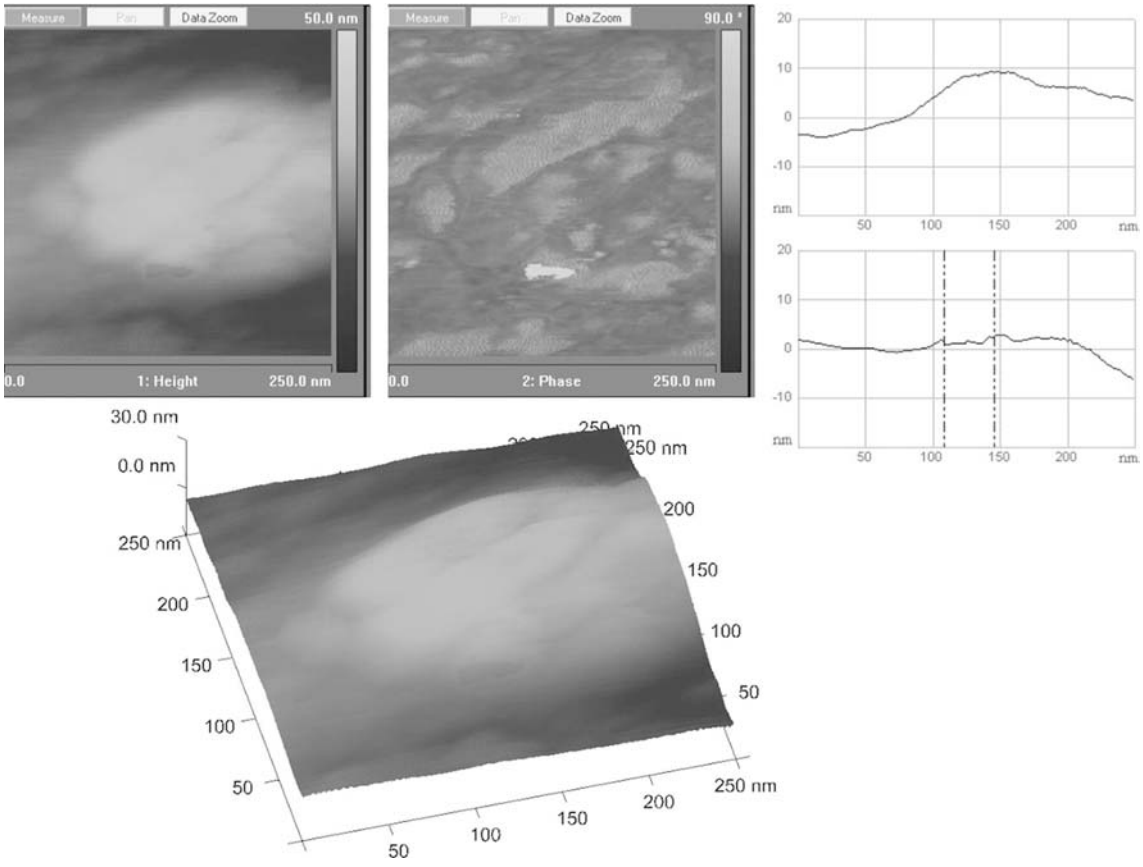

Fig. 7 AFM images of the surface of stainless steel substrates coated with a nitrided NiCr deposit after corrosion in 3% NaCl and CO_2, depicting the early stages of corrosion at the grain boundaries

samples show one maximum point at medium frequencies, attributed to a CPE close to 65°, where an active surface is considered owing to the water content inside the pores of the coating or to breakdown of the corrosion product layer after exposure to 3% NaCl solution.

The corrosion mechanism for the surfaces of the coating is associated with adhesion of the coating to the metallic substrate and the porous layers formed at the surface from corrosion products. For bare carbon steel we obtained the smallest R_{ct} magnitude, 2,400 Ω cm^2, and the highest OCP magnitude, −0.684 V versus the SCE; this is attributed to the metal activation surface owing to chloride ion diffusion through the pores of the iron oxide layer formed and the breakdown of this passive layer that activates the surface of the metal [28]. NiCr9F shows the best corrosion resistant coating in terms of real impedance magnitude (Fig. 8), with an R_{ct} magnitude of 21,960 Ω cm^2.

The nitrogen flow during the sputter deposition and the nitrogen contents in the films control the coating characteristics and the corrosion resistance behavior (Tables 1, 2). When the N_2 gas content in the film is less as in sample NiCr9F (20% N_2–80% Ar), the electrochemical mechanism behaves as a mix phenomenon in terms of charge transfer and mass transfer processes. In this case, the lower nitrogen content and the higher argon content influence the adherence between the film and the substrate, because the coating formed under this environment affects the transport of the ions to the interface between the outer layer and metallic substrate; therefore, charge transfer resistance is higher when the nitrogen content is lower.

NiCr4A and NiCr5F have a higher nitrogen content in the coatings as observed from Table 1. NiCr4A shows an impedance complex diagram with one semicircle, which is attributed either to ionic diffusion throughout the coating layer or to the water content in the coating. This behavior marks the transition from two time constants observed when the coating layer is not water-saturated, like NiCr9H, to one time constant or water-saturated layer observed in NiCr5F or NiCr4A.

Metallic substrates are important to study the corrosion and faradic processes when exposed to aggressive environments like NaCl and NaCl and CO_2; therefore, stainless steel was also examined as a substrate in order to compare corrosion resistance properties of the nitrided NiCr coatings.

Stainless steel was used as a substrate for the nitrided NiCr coatings and was tested under the same electrolyte conditions. Various parameters, like the OCP, R_s, R_{ct}, the CPE and W, were evaluated for all the coatings and are given in Table 3. The impedance signature in Fig. 11a shows that the stainless steel sample (SS) has

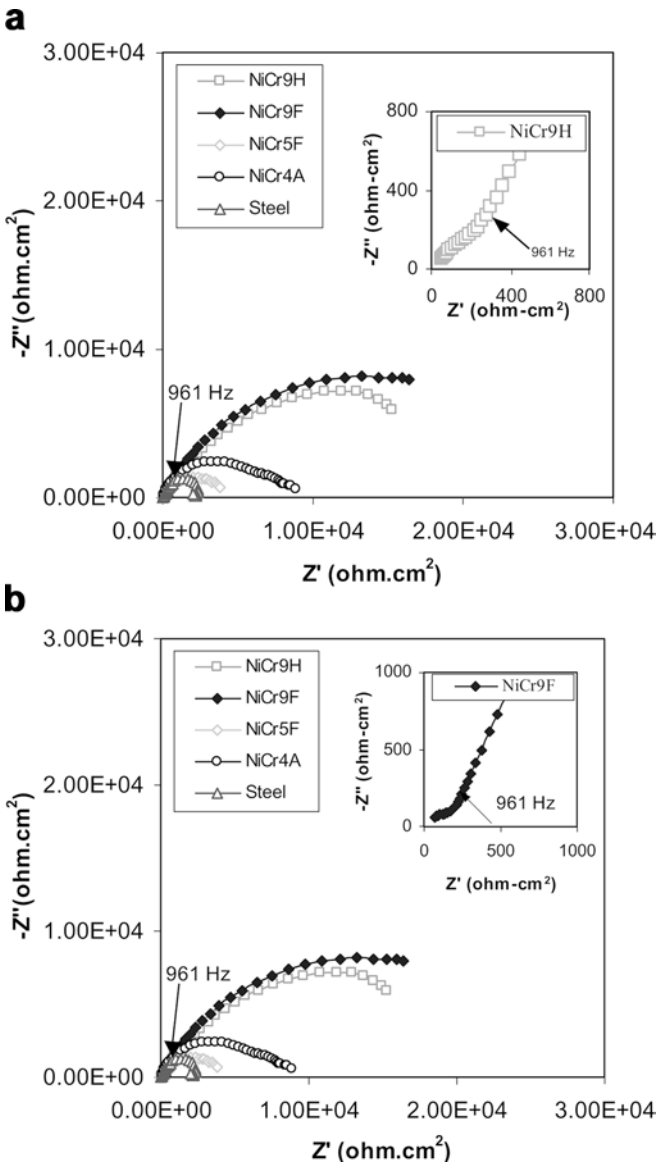

Fig. 8 **a** Impedance signature for different coatings on carbon steel exposed to 3% NaCl. The *inset* shows the amplification at high frequencies for sample NiCr9H. **b** Impedance for different coatings on carbon steel exposed to 3% NaCl, with the *inset* showing the amplification at high frequencies for sample NiCr9F

two different mechanisms, charge transfer and mass transfer when the metallic structure is exposed to brine solution. The Nyquist representation in Fig. 11a shows semicircular behavior for the bare SS characteristic of an activation process, with higher R_{ct}, 101,410 Ω cm^2, than carbon steel samples, 2,400 Ω cm^2, as in Tables 2 and 3. When different coatings with the SS substrate are exposed to brine solution, the mass transfer process controlled the substrate dissolution process. The complex diagram in Fig. 11a shows NiCr9G, NiCr10 and NiCr6 samples under the mass transfer process, where the straight line marks infinite impedance for the complex representation characteristic of a diffusion process [26]. The phase angle diagram in Fig. 12 for NiCr10, NiCr6, NiCr9G and NiCr4B coatings presents two time constants that appear at high and medium frequencies; the high-frequency time constant is related to the coating interface and the medium-frequency constant is related to the metallic structure with electrolyte. Figure 12 shows the phase angle magnitudes are near 60°–70° at medium frequencies. If the magnitude is associated with a pseudo-capacitor with a magnitude near 1×10^{-5} F/cm^2, it can be attributed to good adherence between the substrate and the coating, since the capacitor storage is higher and diffusion and the water content within the coating layer are lower compared with those for the carbon steel substrate.

In terms of the equivalent circuit analogs represented in Fig. 9 for coatings on carbon steel substrates, SS exposed to NaCl solution is described by an active surface or a resistance in series with a parallel capacitor and resistance, R(RC) circuit, illustrated in Fig. 9b. However, the mass transfer process can be attributed to the Warburg impedance parameter associated with a circuit analog like that in Fig. 13. For NiCr4B the coating impedance signal electrical analog represented in Fig. 9b represents the process at the electrode–electrolyte interface: chloride ions and ions that are in solution diffuse throughout the deposited coating and water is present within the coating. The metallic structure is dissolved at a rate equivalent to the diameter of the semicircle in Fig. 11. The magnitude of R_{ct} for the NiCr4B coating is smaller than that of bare stainless steel metal (Tables 2, 3); therefore, the influence of nickel in the coating layer affects the corrosion resistance, making this coating less resistant than chromium oxide at the surface of SS.

NiCr9G, NiCr10 and NiCr6 coatings present a mass transfer control process when a straight line is present in the complex diagram, porous distribution and geometry change impedance characteristics represented in the line angle, electric circuit analog for these samples are similar as represented in Fig. 9a. Phase angle shows two time constants at high and low frequencies associated to the each interface marked in the analog, where high frequency time constant relates coating characteristics, and medium frequency relates electrode–electrolyte characteristics. NiCr9G, NiCr10 and NiCr6 samples show good corrosion resistance, due to the blocking access to aggressive species in the solution throughout the layer that controls mass transport process, therefore charge transfer resistance is improved in these coatings, see Table 3.

OCP magnitudes shown in Table 3 for these samples are nobler than the rest of the previous coatings, marking good physicochemical characteristics of the layers. Porous characteristics for each coating can lead to better corrosion resistance properties, and adherence properties are improved when coating deposition is controlled by argon addition. CO_2 gas was added to the electrolytic solution in order to simulate condensate phase in oil production [16] and test corrosion resistance under this environment.

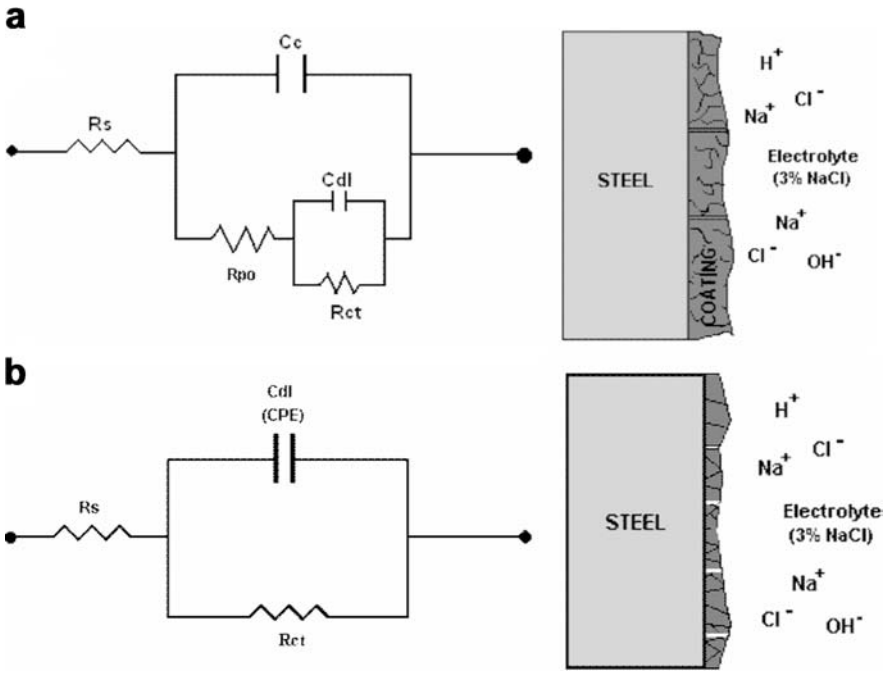

Fig. 9 Equivalent electrical circuit analogs and physical representation of the interface of carbon steel exposed to 3% NaCl solution

Table 2 Open circuit potential (*OCP*) and parameters of the equivalent circuit analog for 3% NaCl when carbon steel is used as a substrate for nitrided NiCr coatings

Sample	OCP (V versus SCE)	R_s (Ω cm^2)	R_{ct} (Ω cm^2)	C_{dl} (F/cm^2)	R_{po} (Ω cm^2)	C_c (F/cm^2)
Carbon steel	−0.684	70	2,400	3.01×10^{-4}	NA	NA
NiCr4A	−0.591	68.69	7,292	3.11×10^{-5}	NA	NA
NiCr5F	−0.673	75.29	3,871	1.38×10^{-4}	NA	NA
NiCr9F	−0.440	78	20,784	1.82×10^{-5}	138	1.85×10^{-7}
NiCr9H	−0.494	73	18,500	1.76×10^{-5}	145	1.03×10^{-7}

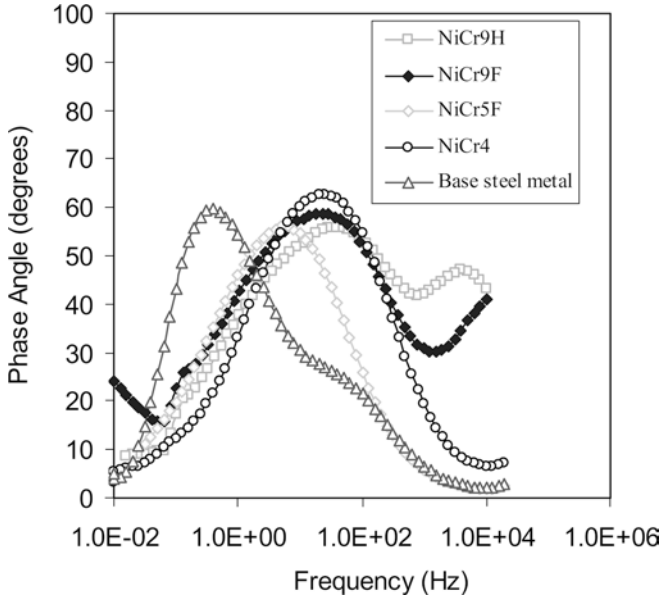

Fig. 10 Impedance signature in the imaginary domain (phase angle) representation for different coatings on a carbon steel substrate exposed to 3% NaCl

Effect of CO_2 addition

Impedance response for NiCr6 coating is illustrated in Fig. 14 when is exposed to NaCl solution and 100 ppm of CO_2(aq) where pH of the solution was 5.35. Nyquist plot represents charge transfer and mass transfer process for different samples. An equivalent circuit analog, like that in Fig. 13, describes the mass transport process for the NiCr6 coating. CO_2(g) dissolved in brine solution forms H_2CO_3 and HCO_3^- at pH 5.35 that diffuse through the deposited layer.

The phase angle response for NiCr9G in Fig. 14 shows two time constants, one for the coating at high frequencies and one for that at medium frequencies that are the contributions of the interface between the electrode and electrolyte. The presence of two time constants confirms the mass transfer process where the coating sets a physical barrier for the diffusion of ions. The electrical circuit analog is similar as given in Fig. 9a describing the interface for this sample. The NiCr10 and NiCr4B coatings and the stainless steel structure show an activation or a charge transfer control process when the complex diagram in Fig. 15 presents semicircular behavior, in this electrolytic solution.

Table 3 OCP and parameters of the equivalent circuit analog for 3% NaCl when stainless steel is used as a substrate for nitrided NiCr coating

Sample	OCP (V versus SCE)	R_s (Ω cm^2)	R_{ct} (Ω cm^2)	CPE-T (F/cm^2)	CPE-P (n)	W-T
Stainless steel	−0.222	43.82	101,410	3.14×10^{-5}	0.84	NA
NiCr4B	−0.175	51.04	56,057	3.23×10^{-5}	0.86	NA
NiCr6	0.185	47.29	83,400	6.81×10^{-6}	0.72	4.5×10^{-4}
NiCr9G	−0.030	49.23	61,098	3.15×10^{-6}	0.82	2.58×10^{-5}
NiCr10	0.070	46.9	41,300	3.64×10^{-6}	0.68	4.12×10^{-4}

The electric circuit analog is considered from Fig. 9b, where the resistance of the electrolyte is R_s, R_{ct} is the charge transfer resistance and C_{dl} is the double-layer capacitance from the electrode–electrolyte interaction. The NiCr4B sample has a smaller charge transfer resistance when it is exposed to the mixture of CO_2 and -NaCl solution compared with NaCl solution (Tables 3, 4); this is attributed to the acidification of the medium, which then is more aggressive against the coating material. Bonding or adherence between the coating and the metallic surface is related to the ionic transfer from the electrolyte to the interface when Cl^- or H_2CO_3 or HCO_3^- accumulates on the pores or at the surface of the metallic structure and starts to acidify the electrolyte-promoting iron dissolution and initiates a failure site that is going to be propagated. The NiCr10 sample

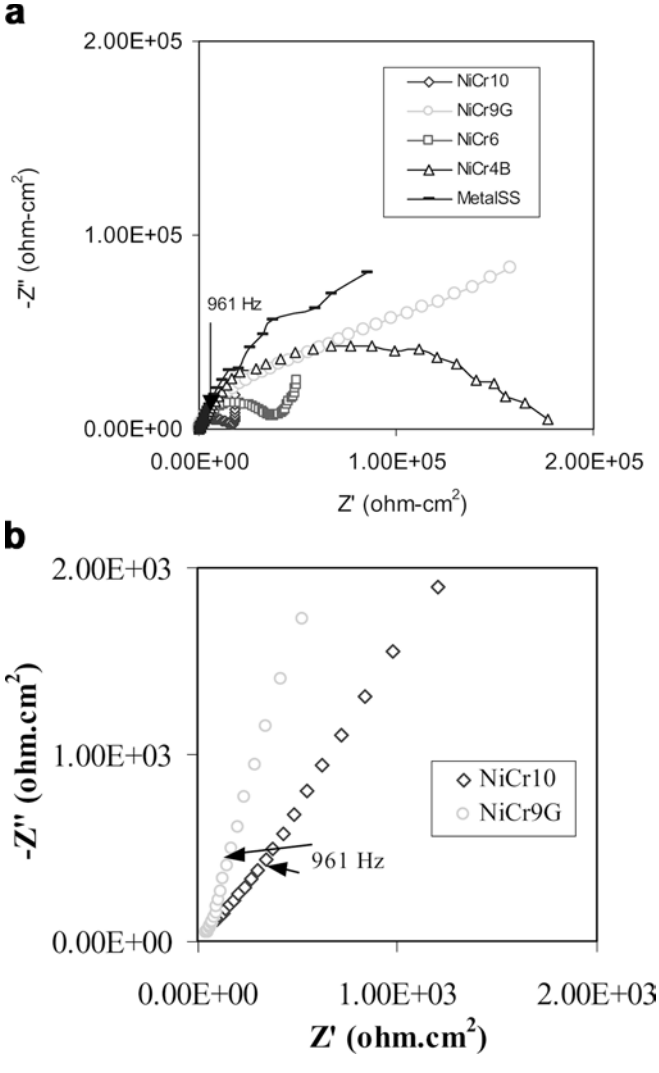

Fig. 11 Impedance signature in the complex representation of different coatings on stainless steel exposed to 3% NaCl with NiCr9H sample amplification at high frequencies

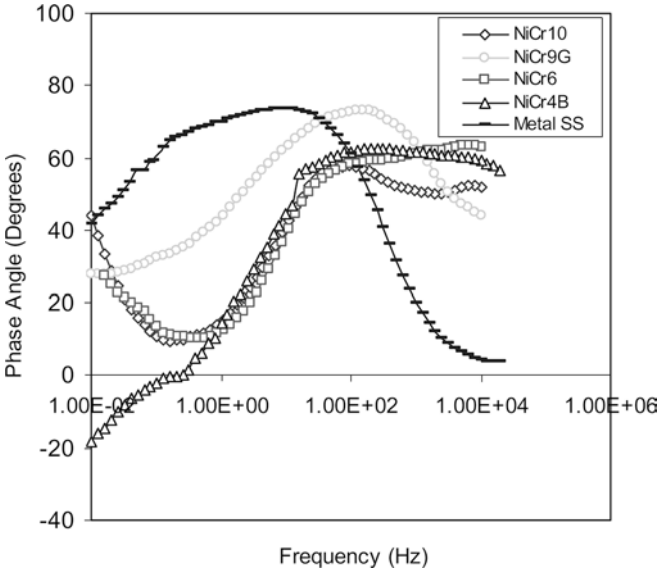

Fig. 12 Impedance signature in the imaginary domain (phase angle) representation for different coatings on stainless steel exposed to 3% NaCl

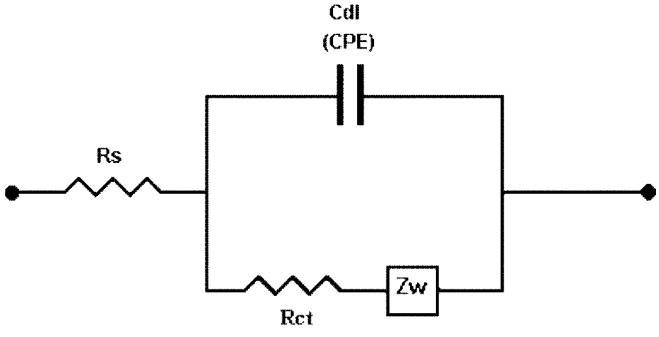

Fig. 13 Equivalent circuit analog of the coating–stainless steel interface exposed to 3% NaCl solution

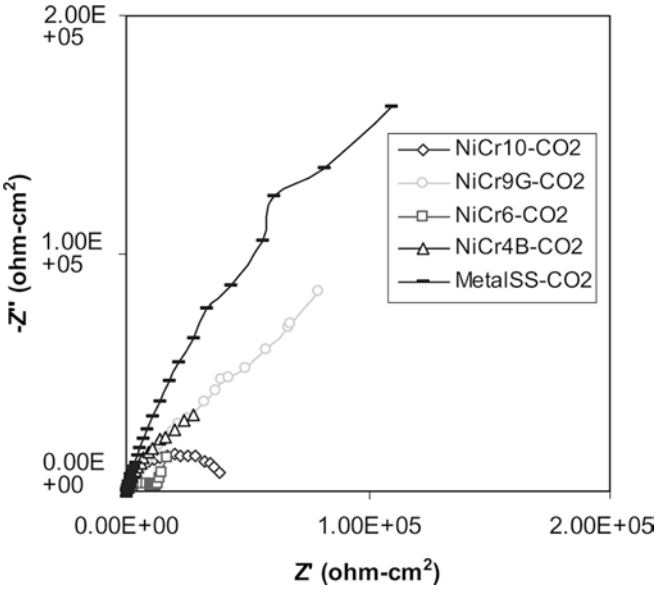

Fig. 14 Impedance signature in the complex representation of different coatings on stainless steel exposed to 3% NaCl and CO_2

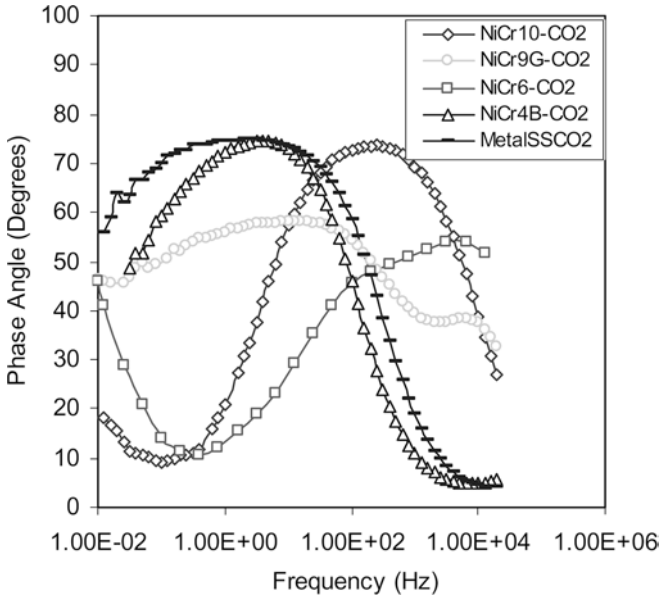

Fig. 15 Impedance signature in the imaginary domain (phase angle) representation for different coatings on stainless steel exposed to 3% NaCl and 100 ppm CO_2(aq)

shows an active mechanism when exposed to the solution mixture; Fig. 15, the magnitude of R_{ct} is finite and C_{dl} is 1.97×10^{-6} F/cm^2.

Figure 16 shows the SEM micrograph of the nitrided NiCr deposits on the carbon steel and on stainless steel. The zones marked I indicate the nitrided NiCr coatings and zones marked II indicate the portions after the corrosion studies. Figure 16a marks different zones after exposure of chloride electrolytic solution; the dark (II) zone shows a pitting attack on the surface of the steel, where the failure initiation took place. Iron oxide as a corrosion product has a heterogeneous porous nature where the ion diffuses through the film changing the pH conditions inside the pores or at the interface of the film–metallic structure. Propagation of the pitting area was considered for steady-state conditions; impedance measurements corroborate metallic dissolution with the charge transfer process observed in the Nyquist representation in Figs. 8 and 9 as described previously with an equivalent circuit. It can be observed that in Fig. 16b there is no attack on the surface of the NiCr9 coating for same chloride solution for the stainless steel substrate. This behavior is attributed to the bonding or adherence of the substrate with a coating as previously described from the equivalent circuit for the mass transfer control process.

Conclusions

Nitrided NiCr thin films were deposited by rf magnetron sputtering at room temperature, using a NiCr composite metal target on well-polished stainless steel and carbon steel substrates under various nitrogen concentrations. Films around 1.2-μm thick were obtained with varying nitrogen concentrations. From the XRD analysis, various structural parameters, like crystallite size, strain and dislocation density, were evaluated. It was found that when the nitrogen concentration increases, the dislocation density and the strain in the films increase. It can also be corroborated that when the nitrogen content increases, the films are more vulnerable to corrosion; this is attributed to the lack of adhesion owing to the dislocation density that promotes more available sites and allows breakdown of the layer. Strain is associated with the dissolution process, since ions in solution diffuse and interact with the interface (coating–surface)

Table 4 Open circuit magnitudes and parameters of the equivalent circuit analog for 3% NaCl and 100 ppm CO_2 when stainless steel is used as a substrate for nitrided NiCr coatings

Sample	OCP (V versus SCE)	R_s (Ω cm^2)	R_{ct} (Ω cm^2)	CPE-T (F/cm^2)	CPE-P (n)	W-T
Stainless steel	−0.051	43.12	337,520	3.58×10^{-5}	0.84	NA
NiCr4B	−0.195	50.6	76,207	5.8×10^{-5}	0.84	NA
NiCr6	0.238	48	11,111	5.84×10^{-6}	0.62	2.64×10^{-4}
NiCr9G	−0.018	46.34	606,470	2.78×10^{-5}	0.60	NA
NiCr10	0.126	40.87	40,941	1.97×10^{-6}	0.84	NA

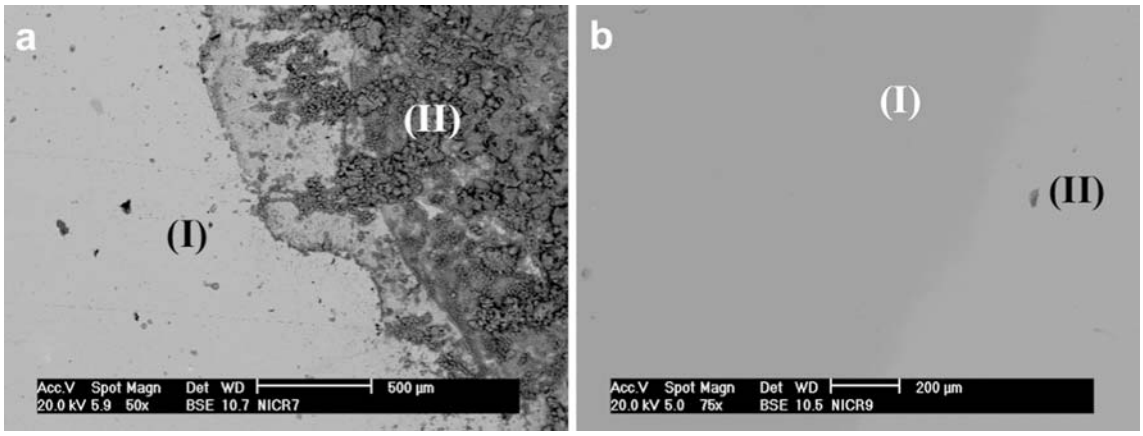

Fig. 16 **a** SEM micrograph of coated (*I*) and corroded (*II*) areas on the carbon steel plates. **b** SEM micrograph of coated (*I*) and corroded (*II*) areas on the stainless steel plates

and the breakdown or lack of adherence can be propagated to the sites where the strain is higher. A more detailed study is needed to determine the influence of the grain size on the corrosion process for a better understanding and control of preferential corrosion sites in the coating materials for developing anticorrosive films and smart sensors. The impedance distribution could follow the corrosion resistance for many coatings by using electrical equivalent circuits and a phenomenological approach by means of the frequency domain technique. Apart from that we conclude that nickel-based coatings on SS substrates can give good corrosion resistance properties depending upon the charge transfer mechanism at the surface. So, the NiCr4B charge transfer mechanism is favored by this environment, making it unsuitable for corrosion resistance applications, but more favorable for coatings on bipolar plates of a fuel cell. But NiCr6 was found to have the best charge transfer mechanism property for corrosion resistance.

Acknowledgements We would like to thank the Mexican Petroleum Institute for financial assistance through project D.00172 and G. Canizal and R. Diaz for the AFM images and E. Sosa for impedance simulation.

References

1. Ak NF, Tekmen C, Ozdemir I, Soykan HS, Celik E (2003) Surf Coat Tech 173:1070
2. Gadenne P, Sella C, Gasgnier M, Benhamou A (1988) Thin Solid Films 165:29
3. Vollaro MB, Potter DI (1994) Thin Solid Films 239:37
4. Mengucci P, Costato M, Majni G (1992) Thin Solid Films 209:67
5. Lim AS, Atrens A (1992) Appl Phys A 54:343
6. Banovec A, Zalar A (1988) Thin Solid Films 164:129
7. Peled A, Farhadyan J, Zloof Y, Baranauskas V (1994) Vacuum 45:5
8. Takeda S (1990) Vacuum 41:1769
9. Nelson JC, Oriani RA (1990) Electrochim Acta 35:1719
10. Hu Y, Tolmachev YV, Scherson DA (1999) J Electroanal Chem 468:64
11. Lesage J, Chicot D, Araujo P, Zampronio M, De Miranda PEV (2000) Thin Solid Films 377:675
12. Li H, Ebrahimi F (2003) Mater Sci Eng A 347:93
13. MacDougall B, Mitchell DF, Graham MJ (1980) J Electrochem Soc 127:1248
14. MacDougall B, Mitchell DF, Graham MJ (1982) Corrosion 38:85
15. Sato N, Kudo K (1974) Electrochim Acta 19:1874
16. Nesic S, Nordsveen M, Nyborg R, Stangeland A (2003) Corrosion 59:6
17. Melendres CA, Pankuch M (1992) J Electroanal Chem 142:103
18. Oblonsky LJ, Devine TM (1995) J Electrochem Soc 142:3677
19. Oblonsky LJ, Devine TM (1995) Corros Sci 37:17
20. Hummel RE, Smith RJ, Verink ED (1987) Corros Sci 27:803
21. Okuyama M, Haruyama S (1974) Corros Sci 14:1
22. Ord JL, Clayton JC, DeSmet DJ (1977) J Electrochem Soc 124:1714
23. Hara N, Sugimoto K (1983) Trans J Inst Metals 24:236
24. Cullity BD (ed) (1956) Elements of X-ray Diffraction. Addison-Wesley, Reading, MA, New York
25. Velumani S, Narayandass Sa K, Mangalaraj D (1998) Semicond Sci Technol 13:1016
26. Taylor S, Gileadi R (1995) Corrosion 51:9
27. Mansfeld F, Tsai T (1993) Corrosion 49:726
28. Park JR, Macdonald DD (1983) Corros Sci 23:4